How to Cite:
Mahmoud, A. A., & Mohammad, J. F. (2022). Study the effect fe doped tin oxide for gas sensing applications. *International Journal of Health Sciences*, *6*(S5), 6380–6390.
https://doi.org/10.53730/ijhs.v6nS5.10125

Study the effect fe doped tin oxide for gas sensing applications

Arshad Ahmed Mahmoud
Physics Department, College of education for pure Sciences, University of Anbar, Iraq

J. F. Mohammad
Physics Department, College of education for pure Sciences, University of Anbar, Iraq
Corresponding author: esp.jamalf.mohamad@uoanbar.edu.iq

***Abstract*---**Nanocrystalline transparent conductive tin dioxide (SnO_2) and Fe doped SnO_2 films were prepared by the chemical spray pyrolysis technique (CSPT). X-ray diffraction (XRD) pattern shows that the SnO_2 films are polycrystalline of tetragonal structure with the preferential orientation of (110) direction and intensity decreases with increasing Fe doping. The results of the film morphology study by SEM show that the films contain nanoparticles with different size distributed on the film. The study of the optical properties reveals that SnO_2 films have high transmittance in the visible region and decrease with Fe doping. The optical energy gaps of the SnO_2 thin films decrease slightly from 3.87 eV to 3.63 eV due to the increase in Fe doping.

***Keywords*---**Tin oxide, Spray pyrolysis, SEM, Doping, Optical Properties.

1. Introduction

Nanocrystalline semiconductors have become the focus of intense research due to their unique physical and chemical properties associated with reduced size and dimensions [1]. Tin dioxide (SnO_2) has high transmittance in the visible region, high conductivity, and wide bandgap (E_g= 3.7 eV) which is employed in various applications such that [2]; solar cells [3,4], gas sensors [5,6], UV photodetectors [7], lithium-ion batteries (LIB) [8], and other optoelectronics devices. Numerous applications need new properties of SnO_2, Which can be achieved through doping with extrinsic different elements such as Li, Cd, Cu, Al, F, Ta, and Sb, which leads to the modification in the electrical and optical properties of the material [9-13]. A wide variety of physical and chemical methods used for the deposition of

pure and doped SnO_2 thin films, including; sol- gel[14], solid-state reaction [15], Chemical Bath Deposition [16], pulsed-laser deposition [17], RF Magnetron sputtering [18], chemical vapor deposition [19] and chemical spray pyrolysis [20,21]. The chemical spray pyrolysis method has the advantages of being efficient, low cost, and used to deposition large surfaces. In the present paper, the influence of Fe doping on some physical properties of tin oxide was investigated.

2. Experimental Part

Nanocrystalline thin films of pure SnO_2 and Fe doped tin oxide (SnO_2) were prepared by the chemical spray pyrolysis technique (CSPT) using stannous chloride ($SnCl_2.2HO_2$) and iron chloride ($FeCl_3$). The tin precursor with 0.02 M dissolved in diluted water (100 ml) using a magnetic stirrer for half an hour, and then, a few drops of hydrochloric acid (HCl) was added to the mixture solution to get high solubility. Microscopic glass slides as substrates (with dimensions 2.5 cm× 2.5 cm) were cleaned with ethanol and distilled water using an ultrasonic bath. The substrate temperature (350 °C), the nozzle height (30cm) were kept constant for each deposition. Finally, the substrates are left for two hours to cool and then kept in special containers.

3. Results and Discussion

3.1 Structural properties (XRD)

Figure (1) shows that the X-ray diffraction (XRD) patterns of nanocrystalline SnO_2 and Fe doped SnO_2 thin films prepared using CSPT. From diffraction patterns, we observe that the prepared films are polycrystalline in nature with broad peaks. A number of Bragg reflections with 2θ values of 26.42º, 33.89º, 38.06º and 54.01º sets of lattice planes are observed which belong to (110), (101), (200) and (211) of tetragonal SnO_2 phase, respectively, (JCPDS card SnO_2, NO. 41-1445). Fe doping tin oxide did not change the tetragonal SnO_2 lattice structure. An increase Fe doping from (1 % to 5 %), the intensity decreases, and no substantial change in the peak position was observed because dopant atoms incorporate homogeneously into the tin oxide matrix. The crystallite size (D) of the pure SnO_2 and SnO_2: Fe particles calculated using the Scherrer formula ($D= k\lambda/\beta\cos\theta$)[22]. The crystallite size is calculated for the prominent peak. The results summarized in Table (1).

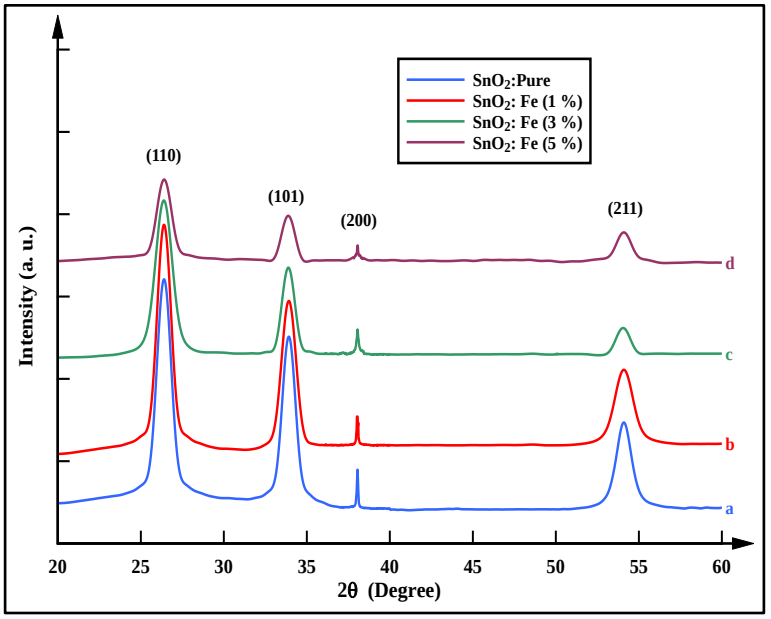

Figure (1): XRD pattern of SnO_2: Fe thin films with different volume percentage of Fe; (a)- pure SnO_2, (b)- 1% Fe, (c)- 3 % Fe and (d)- 5 % Fe

Table 1. XRD results of nanocrystalline SnO_2 and SnO_2:Fe thin films.

Samples	Crystalline size(D)nm	2θ (Degree)	hkl (Tetragonal)	$d_{(hkl)}$ (Å)
SnO_2 Pure	44.6	26.42	110	3.36
SnO_2: Fe 1%	17.3	26.47	110	3.36
SnO_2: Fe 3%	14.5	26.47	110	3.36
SnO2: Fe 5%	6	26.63	110	3.34

3.2 Atomic Force Microscopy (AFM) Results

Surface topography of SnO_2 and SnO_2:Fe thin films examined by AFM. Figure (2) shows three dimensions (3D) atomic force microscopy images of a SnO_2 film doped with Fe (1%, 3%, 5%) prepared at a constant temperature (350 °C) and molar concentration (0.02 M). AFM analysis reveals that the roughness of the prepared film is dependent on the concentration of dopant. The results showed that the morphology of the surfaces of the films is of good uniformity, high surface homogeneity and free of cracks. The doping caused a reduction in the surface roughness (R_S), root mean square (RMS) and average grain size ($D_{average}$) values for all Fe doped tin oxide thin films. The features of these films are useful in optoelectronic applications. The AFM results of the prepared samples are being tabulated in Table (1).

Table 1. AFM results of nanocrystalline SnO_2 and SnO_2: Fe thin films

Sample	RMS (nm)	R_S (nm)	$D_{average}$ (nm)
pure SnO_2	6.56	4.3	38.25
SnO_2: 1% Fe	4.55	3.24	24.41
SnO_2: 3% Fe	3.31	2.46	17.9
SnO_2: 5% Fe	1.49	1.16	8

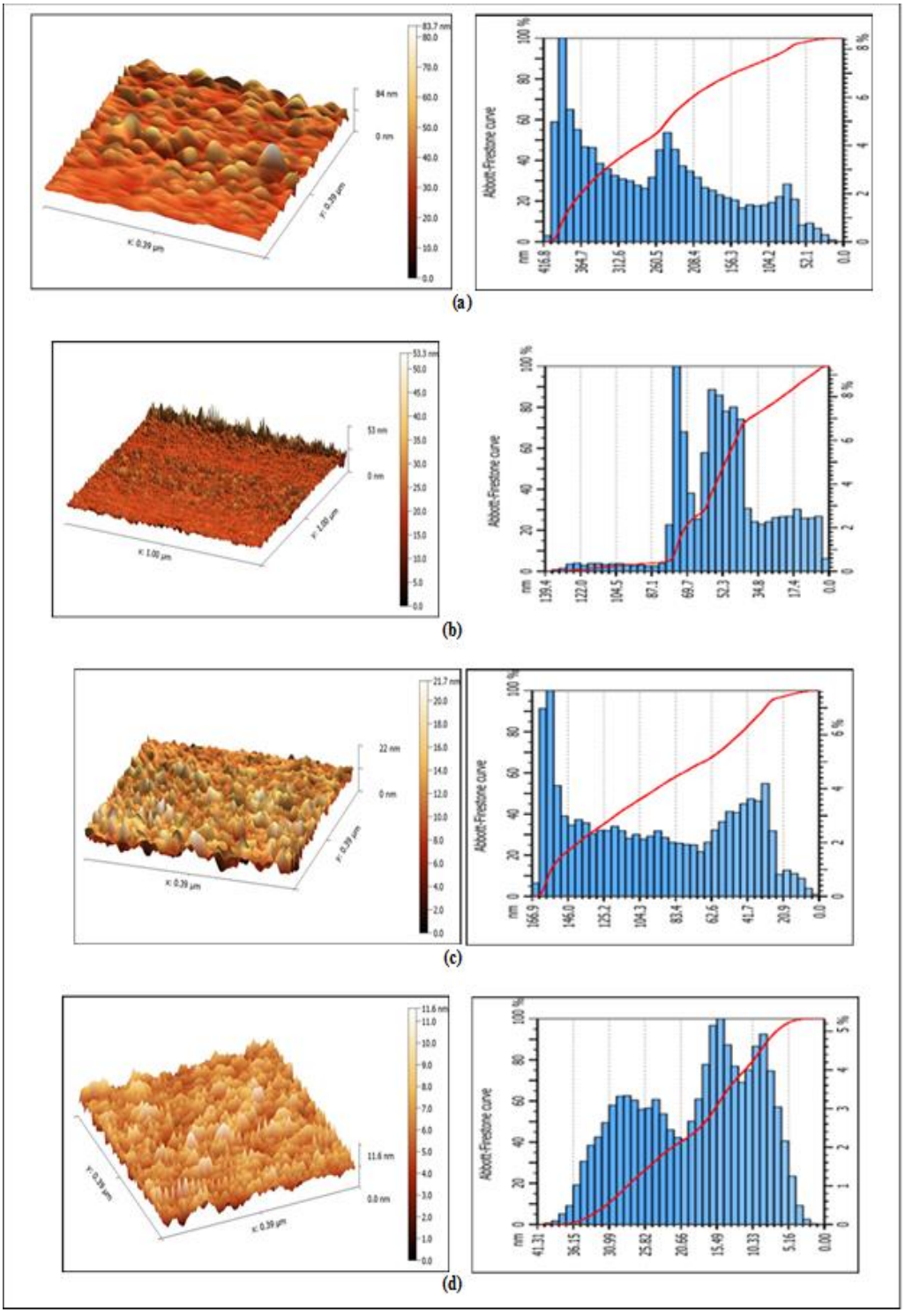

Figure (2): AFM images of; (a)- pure SnO_2, (b)- SnO_2: 1% Fe, (c)- SnO_2: 3 % Fe and (d)- SnO_2: 5 % Fe.

Figure (3) shows scanning electron microscopy (SEM) images of nanocrystalline SnO_2 and SnO_2:Fe films. It is clear that, the morphological properties of the prepared films are affected by doping with different percentages of Fe. The SEM image shows the presence of nanograins and clusters. As the Fe doping increase, the particle size decreased and their shape becomes semi-spherical. The agglomeration of finer grains leads to the formation of flower clusters that have randomly distributed over the surface of the films.

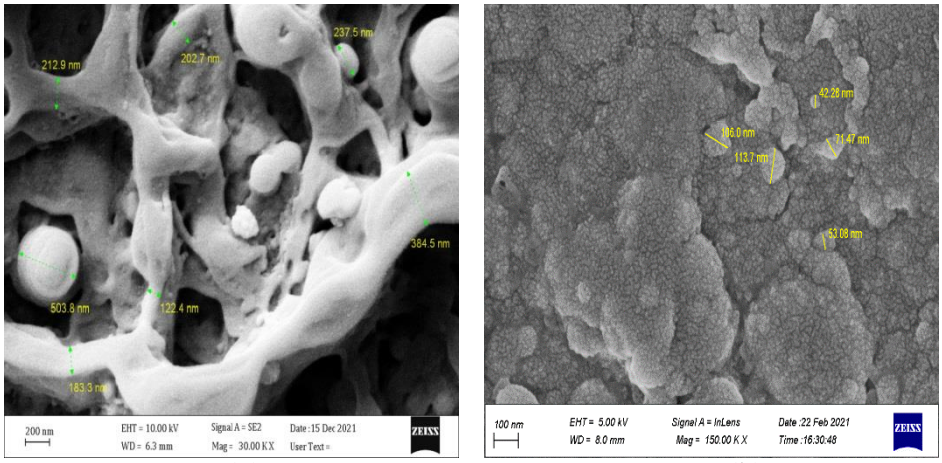

(a) (b)

(c) (d)

Figure (3): SEM images of (a)- pure SnO_2, (b)- SnO_2: 1% Fe, (c)- SnO_2: 3 % Fe and (d)- SnO_2: 5 % Fe.

3.3 Optical Properties Results

Figure (4) shows the optical transmittance spectra of nanocrystalline SnO_2 and Fe doped SnO_2 thin films synthesis using CSPT at temperature 350 ^oC. The undoped SnO_2 film has high transmittance (greater than 70 %) in the visible region of the electromagnetic spectrum. The high transmittance indicates that the SnO_2 film is

free of impurities and has a few lattice defects. The decrease in transmittance with increasing Fe doping possibly attributable to the increase in the thickness of the film with the increase of Fe doping or due to the free carrier absorption of photons. The high transmittance of the transparent conductive oxides (SnO_2), as well as the low resistance, it is of great importance in many electro-optical applications.

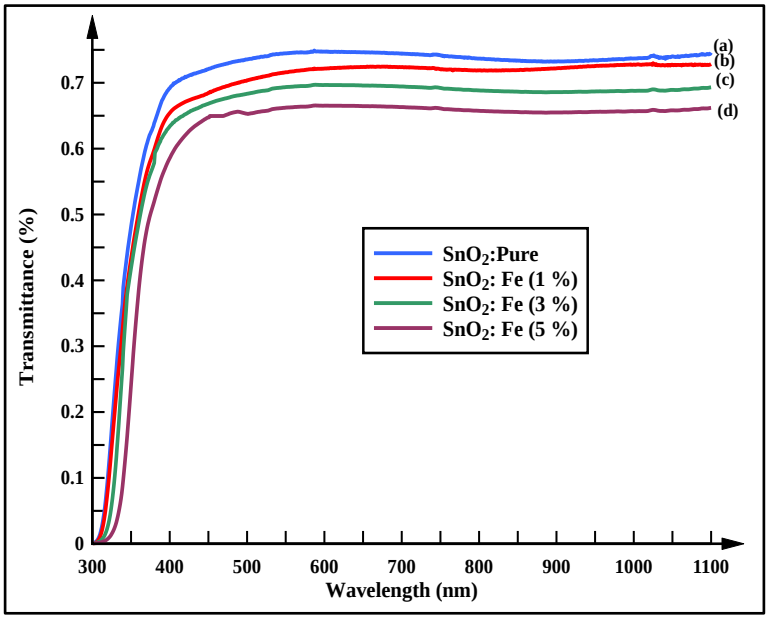

Figure 4: Transmittance versus wavelength of (a) pure SnO_2, (b) SnO_2:1% Fe, (c) SnO_2:3 % Fe and (d) SnO_2:5 % Fe

Figure (5) depicts the optical absorbance (A) spectra of SnO_2 and SnO_2:Fe films grown at 350 ºC at different doping percentages (Fe = 1%, 3% and 5%). The absorption coefficient is found to increase with increasing Fe doping. The increase of (α) can be explained by the fact that the doping which causes creation of donor levels near the conduction band within the energy gap (E_g), which led to the absorption of low-energy photons and thus increased the values of the absorption coefficient.

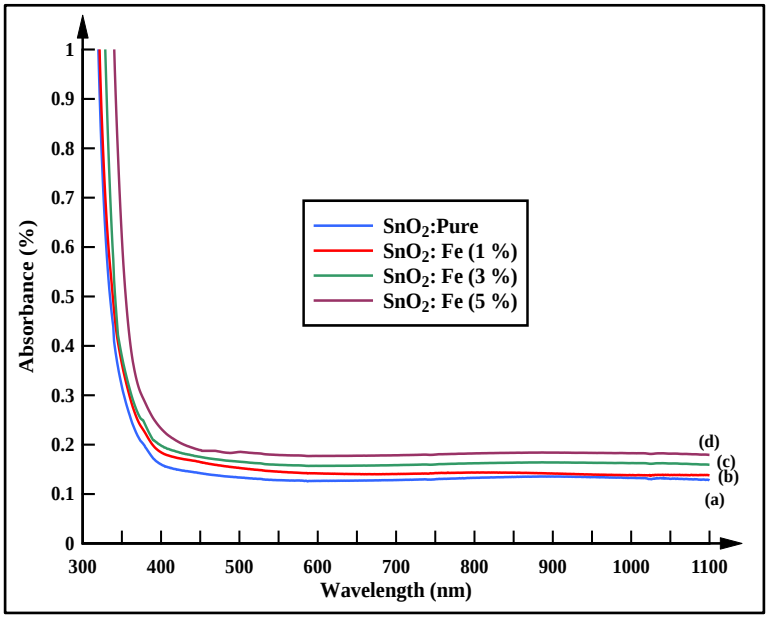

Figure 5: Absorption coefficient versus wavelength of (a) pure SnO_2, (b) SnO_2:1% Fe, (c) SnO_2:3 % Fe and (d) SnO_2:5 % Fe

The absorption coefficient of the allowed transition is related to the energy of the incident photon ($h\upsilon$) by the following equation [23]:

$$(\alpha h\nu) = k\,(h\nu - E_g)^{1/2} \quad \ldots\ldots\ldots\ldots (4)$$

Where (E_g) is the optical bandgap. Figure (6) shows the variation of $(\alpha h\nu)^{1/2}$ as a function of ($h\upsilon$). The optical bandgap of SnO_2 decreases with increasing Fe doping due to the merging of the conduction band and donors' levels. The bandgap (E_g) of SnO_2 is found to be (3.87 eV). This value is greater than of bulk SnO_2 (E_g= 3.6 eV) as a result of the quantum confinement effect (QCE). The value of the bandgap of SnO_2 decreases with an increase in Fe doping. The calculated band gap values for doped SnO_2 with three different Fe doping percentage (Fe = 1%, 3%, 5%) are (3.85, 3.77, and 3.63 eV), respectively. Such a high value of bandgap of films is suitable in optoelectronic applications.

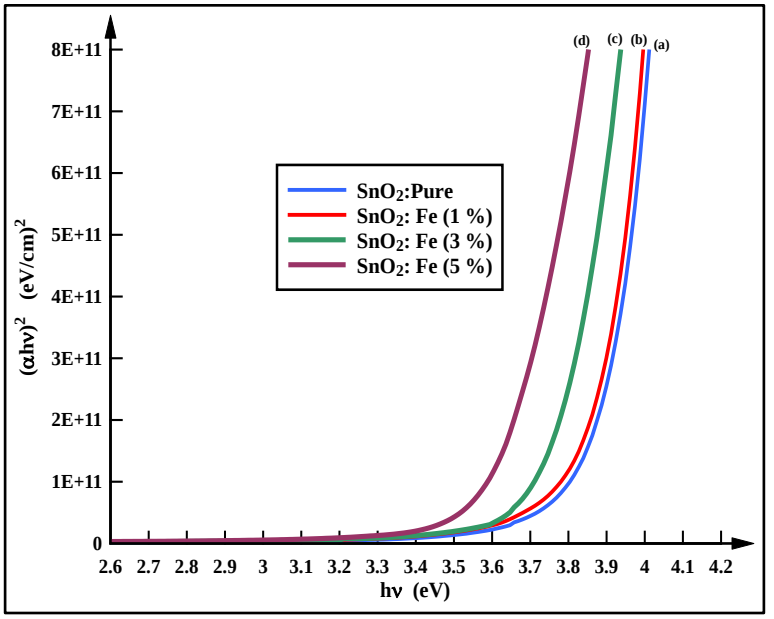

Figure (6): Energy gap of of (a) SnO_2, (b) SnO_2:1% Fe, (c) SnO_2:3 % Fe and (d) SnO_2:5 % Fe

4. Conclusions

Nanocrystalline SnO_2 and Fe doping SnO_2 thin films were successfully synthesized by simple and inexpensive CSPT at a deposition temperature of 350 °C. XRD results confirmed that the prepared films were polycrystalline and tetragonal phases with preferred orientation in the (110) plane. The crystallite size confirms from XRD is 44.6 nm and decreases with Fe doping. AFM analysis reveals that the films are homogeneous, crack-free, and have small roughness. SEM results showed that the SnO_2 films have a nano-particals and the particle size decreases with increasing Fe doping. The SnO_2 films showed high transmittance in the visible region and decreasing by Fe doping. The optical band gap decreases with Fe doping and their values 3.87, 3.85, 3.77, and 3.63 eV corresponding to SnO_2, SnO_2:1% Fe, SnO_2:3 % Fe, and SnO_2:5 % Fe respectively. The Fe doped SnO_2 suitable in the gas sensors device and also for other optoelectronic devices.

Acknowledgment

The authors would like to acknowledge contribution of the University Of Anbar (www.anbar.edu.iq) via their prestigious academic staff in supporting this research with all required technical and academic support

References

[1] N. M. Shaalan, D. Hamad, A. Y. Abdel-Latief, M. A. Abdel-Rahim, Preparation of quantum size of tin oxide: Structural and physical Characterization, Progress in Natural Science: Materials International 26, 145–15,1(2016).

[2] S. G. Onkar, F. C. Raghuwanshi, D. R. Patil, T. Krishnakumar, Synthesis, Characterization and Gas Sensing Study of SnO_2 Thick Film Sensor towards H_2S, NH_3 , LPG and CO_2, Materials Today: Proceedings 23, 190–201, (2020).

[3] S. Chappel, A. Zaban, Nanoporous SnO_2 electrodes for dye-sensitized solar cells: improved cell performance by the synthesis of 18 nm SnO_2 colloids, Solar Energy Materials and Solar Cells, 71, 141–152, (2002).

[4] J. F. Mohammad, M. A. A. Sooud, S M. Abed, Characteristics of pH variation on Structural and optical Properties of nanocrystalline SnO_2 thin films by CBD technique, Journal of Ovonic Research, 16, 107- 113, (2020).

[5] A. Kolmakov, D. O. Klenov, Y. Lilach, S. Stemmer, M. Moskovits, Enhanced gas sensing by individual SnO2 nanowires and nanobelts functionalized with Pd catalyst particles. Nano Lett., 5, 667–673, (2005).

[6] N. V. Duy, N. V. Hieu, P. H. Huy, N. D. Chien, M. Thamilselvan, J.Yi, Mixed SnO_2/TiO_2 Included with Carbon Nanotubes for Gas-Sensing Application. Physica, E 41, 258-263, (2008).

[7] L. Hu, J. Yan, M. Liao, L. Wu, X. Fang, Ultrahigh external quantum efficiency from thin SnO_2 nanowire ultraviolet photodetectors, Small, 7, 1012–1017, (2011).

[8] J. S. Chen, , X. W. Lou, SnO_2- based nanomaterials: Synthesis and application in lithium-ion batteries. Small, 9, 1877–1893, (2013).

[9] Y. Wang, T. Brezesinski, M. Antonietti, B. Smarsly, Ordered mesoporous Sb-, Nb-, and Ta-doped SnO_2 thin films with adjustable doping levels and high electrical conductivity. ACS Nano, 3, 1373–1378, (2009).

[10] Y. Nakano, T. Morikawa, T. Ohwaki and Y. Taga, Band-gap narrowing of TiO_2 films induced by N- doping, Physica B, 376, 823-826, (2006).

[11] B. Stjerna, E. Olsson, C. Granqvist, Optical and electrical properties of radio frequency sputtered tin oxide films doped with oxygen vacancies, F, Sb, or Mo, J. Appl. Phys., 76, 3797–3817, (1994).

[12] K. Sakthiraj, B.Karthikeyan and K. Balachandrakumar, Structural, Optical and Magnetic properties of Copper (Cu) doped Tin oxide (SnO_2) nanocrystal, International Journal of ChemTech Research, 7, 1481-1487, (2015).

[13] G. Zhang, C. Xie, S. Zhang, S. Zhang, Y Xiong, Defect chemistry of the metal cation defects in the p-and n-doped SnO_2 nanocrystalline films, J. Phys. Chem. C, 118, 18097–18109, (2014).

[14] M. R.Vaezi, M. Zameni, The fabrication of a dip- coated tin oxide thin film via sol- gel processing and a study of its gas sensing properties, Journal of Ceramic Processing Research,13, 778-782 (2012).

[15] E. T. H. Tan, G. W. Ho, A. S. W. Wong, S. Kawi, A. T. S. Wee, Gas sensing properties of tin oxide nanostructures synthesized via a solid-state reaction method, Nanotechnology, 19 255706, (2008).

[16] B. Yuliarto, G. Gumilar, D. W. Zulhendri, Nugraha, N. L. W. Septiani, Preparation of SnO_2 Thin Film Nanostructure for CO Gas Sensor Using Ultrasonic Spray Pyrolysis and Chemical Bath Deposition Technique, Vol. 131, 534-538, (2017).

[17] R. Dolbec, M. A. El Khakani, A. M. Serventi, M. Trudeau, R. G. Saint-Jacques, Microstructure and physical properties of nanostructured tin oxide thin films grown by means of pulsed laser deposition, Thin Solid Films, 419, 230–236,(2002).
[18] O. Simionescu, C. Romanit, O. Tutunaru, V. Ion, O. Buiu, A. Avram, RF Magnetron Sputtering Deposition of TiO_2 Thin Films in a Small Continuous Oxygen Flow Rate, Coatings, 9, 442, (2019).
[19] J. Kane, H. Schweizer, W. Kern, Chemical Vapor Deposition of Antimony-Doped Tin Oxide Films Formed from Dibutyl Tin Diacetate, J. Electrochem. Soc., 123, 270–277, (1976).
[20] Suryasa, I. W., Rodríguez-Gámez, M., & Koldoris, T. (2022). Post-pandemic health and its sustainability: Educational situation. International Journal of Health Sciences, 6(1), i-v. https://doi.org/10.53730/ijhs.v6n1.5949
[21] V. Consonni, G. Rey, H. Roussel, B. Doisneau, E. Blanquet, D. Bellet, Preferential orientation of fluorine-doped SnO_2 thin films: The effects of growth temperature. Acta Mater, 61, 22–31, (2013).
[22] S. T. Zhang, J. L. Rouvière, V. Consonni, H. Roussel, L. Rapenne, , E. Pernot, D. Muñoz-Rojas, A Klein, D. Bellet, High quality epitaxial fluorine-doped SnO_2 films by ultrasonic spray pyrolysis: Structural and physical property investigation. Mater. Des., 132, 518–525, (2017).
[23] Fitra, Legowo, D., Utomo, B., Suroto, N. S., Parenrengi, M. A., & Al-Fauzi, A. (2021). Intracranial foreign body granuloma caused by oxidized cellulose polymer and etherified sodium carboxymethyl cellulose: an experimental study with orictolagus cuniculus rabbits. International Journal of Health & Medical Sciences, 4(2), 267-272. https://doi.org/10.31295/ijhms.v4n2.1741
[24] G. W. Scherer, “Recent Progress in Drying of Gels”, Journal of Non-Crystalline Solids 147-148, 363-374, (1992).
[25] J. F. Mohammad, S. M. Abed, Preparation and characterization of aluminum-doped nanocrystalline zinc oxide for solar cells applications, Journal of Ovonic Research, Vol. 15, No. 1, pp. 61 – 67, (2019).